

# Quantum Control of Photodissociation by Manipulation of Bond Softening

Adi Natan,<sup>1,\*</sup> Uri Lev,<sup>2,\*</sup> Vaibhav S. Prabhudesai,<sup>1,\*</sup> Barry D. Bruner,<sup>1</sup> Daniel Strasser,<sup>3</sup>  
Dirk Schwalm,<sup>4</sup> Itzik Ben-Itzhak,<sup>5</sup> Oded Heber,<sup>2</sup> Daniel Zajfman,<sup>2</sup> and Yaron Silberberg<sup>1</sup>

<sup>1</sup>*Department of Physics of Complex Systems, Weizmann Institute of Science, Rehovot 76100, Israel*

<sup>2</sup>*Department of Particle Physics and Astrophysics,*

*Weizmann Institute of Science, Rehovot 76100, Israel*

<sup>3</sup>*Institute of Chemistry, Hebrew University, Jerusalem 91904, Israel*

<sup>4</sup>*Max-Planck-Institut für Kernphysik, Heidelberg 69117, Germany*

<sup>5</sup>*J. R. Macdonald Laboratory, Department of Physics,  
Kansas State University, Manhattan, Kansas 66506, USA*

We present a method to control photodissociation by manipulating the bond softening mechanism occurring in strong shaped laser fields, by varying the chirp sign and magnitude of an ultra-short laser pulse. Manipulation of bond-softening is experimentally demonstrated for strong field (795 nm,  $10^{12} - 10^{13}$  W/cm<sup>2</sup>) photodissociation of H<sub>2</sub><sup>+</sup>, exhibiting substantial increase of dissociation by positively chirped pulses with respect to both negatively chirped and transform limited pulses. The measured kinetic energy release and angular distributions are used to quantify the degree of control of dissociation. The control mechanism is attributed to the interplay of dynamic alignment and chirped light induced potential curves.

PACS numbers: 82.50.Nd, 33.80.-b, 82.50.Pt

Controlling chemical processes using laser pulses has been a long standing goal of scientists in physics and chemistry. Much effort has been directed in recent years towards achieving efficient photodissociation via quantum coherent control. One commonly used approach is based on self-learning techniques, in which an optimal pulse shape is found through various iterative optimization procedures [1]. However, while learning algorithms have been successful in producing effective control fields, the physical mechanisms underlying this control are still generally difficult to interpret. Another category of control schemes involve adiabatic population transfer methods, where chirped pulses are used in order to efficiently populate an excited level [2], or to control dissociative ionization [3–5]. Yet a different approach is to employ a pump-probe scheme, where a typical time scale of the system, such as the vibrational period, is used in controlling the outcome [6–10]. Here, we demonstrate how light-matter interaction can be harnessed to achieve control using the bond softening mechanism.

The interaction of molecules with strong fields can be represented by the Floquet dressed state formalism [11]. For the case of diatomic molecules with bound and repulsive potential curves, like H<sub>2</sub><sup>+</sup>, the interaction of light with the molecule shifts down the energy of the upper, repulsive potential curve by  $\hbar\omega$ , where  $\omega$  is the frequency of the laser. The new diabatic potential curves now cross at an internuclear distance where the two electronic states are resonantly coupled by the laser field (Fig. 1). As the laser intensity increases an avoided crossing opens at the resonant internuclear separation, and in addition, the molecule starts to dynamically align with the field polarization. Such excitation fields can then be sufficient to

cause bound population to cross the barrier and dissociate, in a processes known as bond softening [12]. This adiabatic picture can be used as long as the pulse duration is not shorter than the molecular vibration time-scale [13].

Previous studies that used such phenomena to control photodissociation employed a pump-probe scheme. This technique often required a precursor molecule in order to launch a vibrational wave packet on the ground state of the target molecular ion. The control of photodissociation depended on precisely timing the wave-packet motion to the crossing point where the gap opens. This timing was usually controlled by varying the time delay between a strong pump pulse that excites a wave-packet, and a ‘control’ pulse that is responsible for creating the avoided crossing [6–8]. In contrast to this approach, we show that it is possible to control strong field photodissociation by manipulation of the avoided crossing using intense shaped pulses, and without the need of an initial wave-packet preparation.

We focus on one of the most studied molecular systems, H<sub>2</sub><sup>+</sup>. This simple system has revealed remarkably rich dynamics such as bond hardening, bond softening and above threshold dissociation [11–16]. For H<sub>2</sub><sup>+</sup> only the two lowest-lying potential surfaces,  $1s\sigma_g$ , and  $2p\sigma_u$ , need to be considered for the field intensities used in this experiment. Bond softening can be described by diagonalizing the molecule-field Hamiltonian in the Floquet picture [11] (see Fig. 1):

$$E_{\pm} = \frac{V_g + V_u - \hbar\omega}{2} \pm \frac{1}{2} \sqrt{(V_g + \hbar\omega - V_u)^2 + 4V_{gu}^2}, \quad (1)$$

where  $V_g$  and  $V_u$  are the molecular potential energies of the  $1s\sigma_g$  and  $2p\sigma_u$  states,  $V_{gu} = -\frac{1}{2}\varepsilon(t)D(R)\cos\theta(t)$  is the coupling term between them with the transition dipole moment  $D(R)$ ,  $\theta(t)$  is the angle of the molecular

\* These authors have equal contribution.

axis with respect to the laser polarization, and  $\varepsilon(t) = A(t) \cos[\omega(t)t]$ , where  $A(t)$  is the temporal envelope with instantaneous frequency  $\omega(t)$ . The properties of the avoided crossing are thus governed by the field intensity, frequency, and the degree of molecular alignment with respect to the laser polarization. The temporal evolution of molecular alignment results in a change of the angular distribution of the molecules, and is dependant on the intensity of the excitation pulse [17].

Dynamically modifying the avoided crossing can therefore be used to control dissociation. The position of the avoided crossing depends on  $\hbar\omega(t)$ . For example, positively chirped pulses will displace the avoided crossing according to the direction of the frequency sweep, from red to blue-detuned frequencies. The chirp rate corresponds to the displacement rate of the avoided crossing, the longer the pulse the slower the frequency sweep. The gap at the avoided crossing is proportional to  $V_{gu}$  and becomes larger for increasing  $A(t)$  and  $\cos\theta(t)$ . In addition,  $\cos\theta(t)$  significantly increases as the field amplitude peaks, but only slightly decreases afterwards [17, 18]. Thus, for typical symmetric temporal envelopes such as gaussian pulses, the energy gap at the avoided crossing will be larger at  $t_0 + \Delta t$  than at  $t_0 - \Delta t$ , where  $t_0$  the time of peak amplitude, and  $\Delta t$  is some positive time delay. Specifically for positively chirped pulses, the avoided crossing at the temporal peak of the pulse will be larger for blue-detuned frequencies than for red-detuned ones, promoting dissociation of levels below the crossing (Fig. 1 inset). For negatively chirped pulses however, the dynamic displacement raises the effective barrier and suppresses dissociation of these levels.

We examined photodissociation of  $\text{H}_2^+$  as the target molecule experimentally by focusing 30 fs pulses at 795 nm central wavelength (peak intensities  $\leq 2 \times 10^{13}$  W/cm<sup>2</sup>) on a well collimated pulsed 4 keV  $\text{H}_2^+$  ion beam. The molecules were in a rotationally excited Franck-Condon distribution of vibrational states. Both neutral H and proton fragments of the molecular ion were measured in coincidence using a time and position sensitive detector comprised of a phosphor screen anode attached to a microchannel plate with a CCD camera and a home-build frame grabber. The full 3D momentum components for each event were reconstructed from the measured positions and times of flight. From these momentum components, we deduced the kinetic energy release (KER) upon dissociation and the angle  $\theta$  between the molecular axis and the laser polarization at the time of dissociation. Post-dissociation rotations were neglected as the experimental parameters were within the axial recoil approximation [18]. The pulse shaping was performed using a conventional 4-f phase-only pulse shaper [19]. Further details regarding the experimental system were recently described elsewhere [20]. Using the pulse shaper, we applied a quadratic spectral phase function,  $\Phi(\omega) = \phi''(\omega - \omega_0)^2/2$ , where  $\phi''$  is the group dispersion delay (GDD) parameter, which corresponds to the chirp magnitude, and  $\omega_0$  is the central laser frequency.

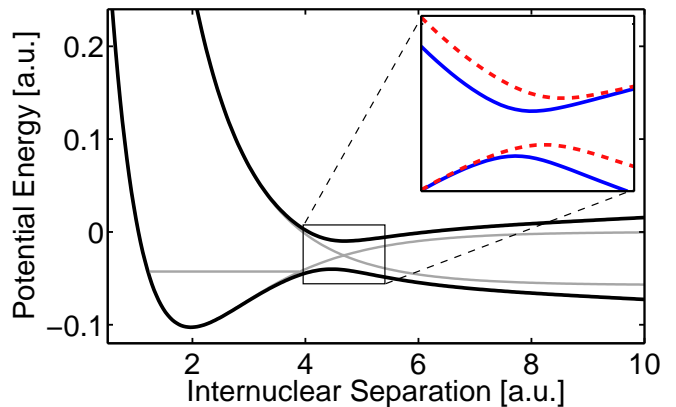


FIG. 1. (color online)  $\text{H}_2^+$  adiabatic potential curves. As intensity increases, the adiabatic (black) light induced potential curves are modified and an avoided crossing opens at the resonant internuclear separation, causing dissociation for levels such as  $v = 7$  (orange). The diabatic potential curves (grey) show the position of the crossing. (inset) For positively chirped pulses, the adiabatic potential curves are dynamically modified from red (dashed red) to blue (solid blue) shifted potential curves, according to the direction of the frequency sweep. A larger gap size for blue-detuned frequencies develops as the temporal alignment evolves close to peak intensity.

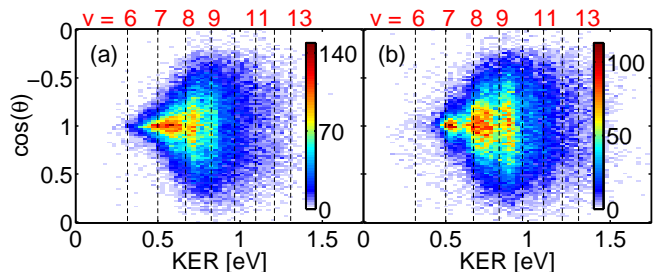


FIG. 2. (color online)  $\cos\theta$  vs kinetic energy release (KER) spectra of  $\text{H}_2^+$  photodissociation by (a) positively chirped and (b) negatively chirped pulses of 90 fs duration (GDD =  $\pm 920$  fs<sup>2</sup>, peak intensity of  $I_0 = 7 \times 10^{12}$  W/cm<sup>2</sup>). Vertical dotted lines indicate the expected peak positions of different vibrational levels at the central wavelength of the laser (795nm).

The pulse shaper was also used to accurately compensate higher orders of dispersion that can arise from downstream optical elements. During the experiments the sign and magnitude of the chirp were alternated every three minutes in order to avoid possible long term drift biases in the measurements.

We measured the KER spectra for pulses with GDD values ranging from -1920 to +1920 fs<sup>2</sup>. This resulted in negatively and positively chirped pulses of durations of 30 fs (transform limited) to 180 fs, of the same bandwidth and fluence. Fig. 2(a-b) show density plots of the distribution of dissociation events as a function of

$\cos\theta$  and KER for 90 fs (GDD of  $\pm 920$  fs<sup>2</sup>) positively and negatively chirped laser pulses, respectively. There are key differences between the KER spectra for the two chirp signs. First, we resolve energetic shifts of KER peaks that result from the temporal ordering of frequencies in the chirped pulse [20]. Second, we note significant changes in the angular distributions and signal strengths in the KER region below 0.7 eV. These changes reflect the different character of the dissociation mechanism for the field intensity used. Vibration levels that are located close to the one-photon crossing, as in the case of  $v = 9$ , are expected to dissociate at the leading edge of the pulse [20], with angular distributions of  $\cos^2\theta$ . This distribution indicates that a resonant one-photon transition occurred and that no alignment took place [15, 21]. However, dissociation from lower levels, such as  $v = 7$ , show narrower angular distributions that can be expressed by higher cosine powers [15, 22], reflecting geometric or dynamic alignment. We label such non-resonant dissociation events as ‘Over the Barrier Dissociation’ (OBD).

We used the angular distribution information to separate the OBD contribution from the near-resonant dissociation events. This approach was taken to avoid the KER shifts effect that arise in near-resonant dissociation events for different chirp magnitudes [20]. The vibration level that is nearest to resonance with the laser is  $v = 9$ , whereas  $v = 7$  has no overlap with the laser bandwidth, hence can dissociate only via OBD. Therefore, measuring dissociation from these levels are appropriate examples for the controllability of OBD and near-resonant dissociation. For example, in Fig. 3(a) we present two angular distributions due to a 90 fs positively chirped pulse of GDD=920 fs<sup>2</sup>, that relate to levels  $v = 9$  and  $v = 7$ , for which KER=0.74 $\pm$ 0.02 and 0.54 $\pm$ 0.02 eV, respectively. A cosine power series function of the form:  $f(E, \theta) = \sum_n a_n(E) \cos^{2n}\theta$  was fitted to the measured angular distributions for the given KER values. Having the fit factors  $a_n(E)$ , we calculated the relative contribution of the  $n^{\text{th}}$  term for a given KER by  $W_n(E) = \int \frac{a_n(E) \cos^{2n}\theta}{f(E, \theta)} d\cos\theta$ . We found that  $n = 4$  is the minimal power required to obtain an accurate fit. Near-resonant dissociation contribution will be therefore expressed by  $W_1$ , and OBD contribution by  $W_{n \geq 2}$ . The molecular degree of alignment during dissociation is also extracted from the measured angular distributions using the expectation value  $\langle \cos^2\theta \rangle = \sum P_i \cos^2(\theta_i) / \sum P_i$ , where  $P_i$  is the measured distribution and  $-\pi/2 \leq \theta_i \leq \pi/2$ . For a pure  $\cos^2\theta$  distribution  $\langle \cos^2\theta \rangle = 0.75$ , whereas for a  $\cos^8\theta$  distribution  $\langle \cos^2\theta \rangle = 0.9$ .

The fitting procedure was used to analyze the angular distribution of the entire KER spectra for different chirp magnitudes up to  $\pm 1920$  fs<sup>2</sup>. For example, in Fig. 3(b-c) we project all dissociation angles on the KER axis for positively and negatively chirped pulses of GDD =  $\pm 920$  fs<sup>2</sup>. The  $W_1$  contribution (blue areas) is similar for the two chirp signs, with about 10% difference. However,  $W_{n \geq 2}$  (red areas) contribution show 70% more OBD for +920 fs<sup>2</sup> than for -920 fs<sup>2</sup>. The overall number of near-

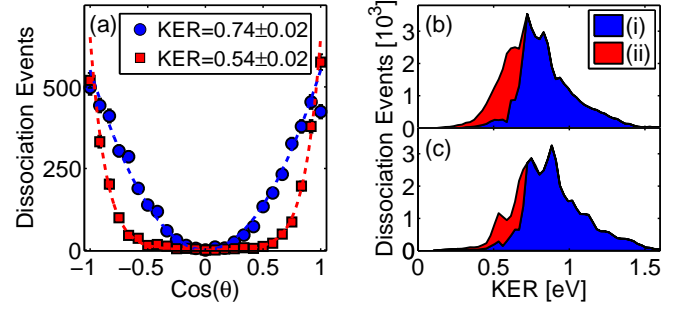


FIG. 3. (color online) Analyzing dissociation angular distributions. (a) Angle vs dissociation events for specific KER values of  $\text{H}_2^+$  from positively chirped pulses (GDD=920 fs<sup>2</sup>) and the corresponding fit function. For KER=0.54 eV a  $\cos^8\theta$  distribution is found suggesting OBD, whereas for KER=0.74 eV a  $\cos^2\theta$  distribution is found suggesting near-resonant dissociation. (b) The entire KER spectra for GDD=+920 fs<sup>2</sup> and (c) GDD=-920 fs<sup>2</sup>. The  $W_{n \geq 2}$  contribution (red area) associated with OBD is 70% larger in positively chirped pulses than negatively chirped pulses, whereas  $W_1$  contribution (blue area) differs only by 10% (see text).

resonant and OBD events was then extracted for different chirp magnitude, as shown in Fig. 4(a). For near-resonant dissociation we obtain less than 10% variation in dissociation rate, although the peak intensity changes by a factor of six for different chirp magnitudes. This finding supports the assumption that the fragments measured with  $\cos^2\theta$  angular distributions ( $W_1$ ) were dissociated mostly by resonant one-photon transitions, and therefore were insensitive to the different peak intensities of the pulses. OBD events that have narrower angular distributions ( $W_{n \geq 2}$ ) are found to be markedly dependent on the chirp magnitude and sign, with approximately 100% variation.

Dissociation from positively chirped pulses in the range 500-1200 fs<sup>2</sup> is found to be more efficient than from transform limited pulses. Chirped pulses with GDD=1320 fs<sup>2</sup> (120 fs duration) produce a nearly equal number of OBD events compared with transform limited pulses, even though the peak intensity is smaller by a factor of four. At GDD values higher than 1320 fs<sup>2</sup>, the number of OBD events diminishes due to the decreasing peak intensity inherent to exceedingly elongated pulses. In order to neutralize the influence of peak intensity on the efficiency of dissociation, one can examine the ratio of positive to negative chirp dissociation events of the same chirp magnitude, hence the same peak intensity. At 1600 fs<sup>2</sup>, for example, we find that positively chirped pulses induce dissociation up to 55% more efficiently than negatively chirped pulses, whereas near-resonant dissociation events are barely affected by the sign of the chirp.

To conclude, we have demonstrated that strong field photodissociation of  $\text{H}_2^+$  is controllable by varying the sign and magnitude of a linearly chirped intense ultra-

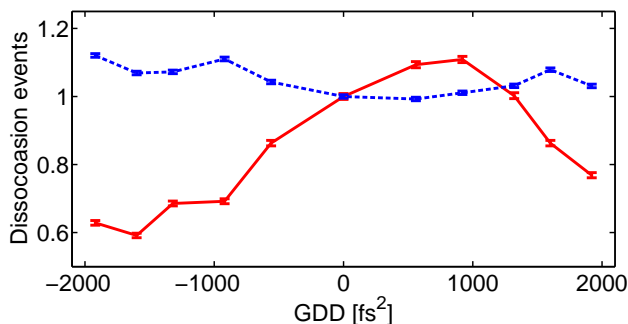


FIG. 4. (color online) Controlling OBD dissociation events. For OBD (solid red), positive chirp is more efficient than negative chirp (Events normalized to zero chirp), whereas near-resonant dissociation (dash blue) is less affected by different chirp magnitudes.

short pulse. We suggest a simple mechanism to explain this control, using a dynamic dressed potential curves picture. This approach enhances or suppresses photodissociation where bound-to-repulsive transitions dominate. Linear chirp is not necessarily the optimal pulse shape that controls dissociation, as higher orders of dispersion can be used to optimally tailor the instantaneous frequency and intensity envelope. Future experiments, for example, could combine third order dispersion with GDD to yield asymmetric temporal envelopes with frequency sweeps that may further enhance dissociation.

We thank B. D. Esry, and N. Moiseyev for helpful discussions. This work was partially supported by the Israeli Science Foundation, the Chemical Sciences, Geosciences, and Biosciences Division, Office of Basic Energy Sciences, Office of Science, US Department of Energy, and the U.S.-Israel Binational Science Foundation (BSF).

- 
- [1] R. S. Judson and H. Rabitz, Phys. Rev. Lett. **68**, 1500 (1992); A. Assion *et. al.*, Science. **282**, 919 (1998) ; T. C. Weinacht, J. Ahn and P. H. Bucksbaum, Nature **397**, 233 (1999).
  - [2] S. Chelkowski, A. D. Bandrauk and P. B. Corkum, Phys. Rev. Lett. **65**, 2355 (1990); B. W. Shore, K. Bergmann, J. Oreg and S. Rosenwaks, Phys. Rev. A **44**, 7442 (1991).
  - [3] L. J. Frasinski *et. al.*, Phys. Rev. Lett. **83**, 3625 (1999).
  - [4] H. G. Breunig, A. Lauer and K. M. Weitzel, J. Phys. Chem. A **110**, 6395 (2006).
  - [5] K. P. Singh *et. al.*, Phys. Rev. Lett. **104**, 023001 (2010).
  - [6] H. Niikura, P. B. Corkum, and D. M. Villeneuve, Phys. Rev. Lett. **90**, 203601 (2003).
  - [7] H. Niikura, D. M. Villeneuve, and P. B. Corkum, Phys. Rev. Lett. **92**, 133002 (2004).
  - [8] B. J. Sussman, D. Townsend, M. Y. Ivanov, and A. Stolow, Science **314**, 278 (2006).
  - [9] Th. Ergler *et. al.*, Phys. Rev. Lett. **97**, 193001 (2006).
  - [10] F. Kelkensberg *et. al.*, Phys. Rev. Lett. **103**, 123005 (2009).
  - [11] A. Giusti-Suzor, F. H. Mies, L. F. DiMauro, E. Charron and B. Yang, J. Phys. B: At. Mol. Opt. Phys. **28**, 309 (1995).
  - [12] P. H. Bucksbaum, A. Zavriyev, H. G. Muller, and D. W. Schumacher, Phys. Rev. Lett. **64**, 1883 (1990).
  - [13] J. H. Posthumus, Rep. Prog. Phys. **67**, 623 (2004).
  - [14] I Ben-Itzhak *et. al.*, Phys. Rev. Lett. **95**, 073002 (2005).
  - [15] K. Sändig, H. Figger, and T. W. Hänsch, Phys. Rev. Lett. **85**, 4876 (2000).
  - [16] J. McKenna *et. al.*, Phys. Rev. Lett. **100**, 133001 (2008).
  - [17] M. Uhlmann, T. Kunert, and R. Schmidt, Phys. Rev. A **72**, 045402 (2005).
  - [18] F. Anis, T. Cackowski, and B. D. Esry, J. Phys. B: At. Mol. Opt. Phys. **42**, 091001 (2009).
  - [19] A. M. Weiner, Rev. Sci. Instrum. **71**, 1929 (2000).
  - [20] V. S. Prabhudesai *et. al.*, Phys. Rev. A, **81**, 023401 (2010).
  - [21] I. D. Williams *et. al.*, J. Phys. B **33**, 2743 (2000).
  - [22] P. Q. Wang *et. al.*, J. Phys. B **38**, L251 (2005).